

## Progradational sand-mud deltas in lakes and reservoirs. Part 2. Experiment and numerical simulation

### Formation des deltas de sable et de boue dans les lacs et les réservoirs. 2<sup>ème</sup> Partie. Expérience et simulation numérique

SVETLANA KOSTIC and GARY PARKER, *St. Anthony Falls Hydraulic Laboratory, University of Minnesota, Minneapolis, MN, 55414, USA*

#### ABSTRACT

Rivers deposit deltas wherever they reach standing water, i.e. a lake or reservoir. Here the case of a sand-bed river carrying mud as wash load is considered. In general the sand tends to deposit out to form a fluvial topset and an avalanching foreset, and the mud tends to deposit out as a bottomset. During floods, many sand-bed rivers carry sufficiently high concentrations of washload to render the river water heavier than that of the body of standing water. In such a case the mud-laden river flow plunges to form a bottom turbidity current. In a companion paper a 1-D numerical model of a prograding delta was presented. In this model fluvial, avalanching and turbidity current deposition are all linked in terms of a moving boundary formulation. Here the model is compared against two experiments on delta progradation. The experiments reveal an intriguing interaction between the three elements of the model, with foreset progradation burying the bottomset and pushing its upstream point ever downstream, and with bottomset deposition raising the toe of the foreset, so increasing the rate of foreset progradation as sand is delivered from the topset. The numerical model of the companion paper captures this interaction with a minimum of adjustment of input parameters. The resulting description of delta morphodynamics is very similar to that observed in e.g. the delta in the Colorado River, USA where it reaches Lake Mead.

#### RÉSUMÉ

Les rivières déposent des deltas à chaque fois qu'elles atteignent de l'eau calme, c'est-à-dire un lac ou une retenue. Ici, on considère le cas d'un lit sableux de rivière transportant de la boue comme charge de lessivage. En général, le sable tend à se déposer pour former une couche fluviale au sommet et un dépôt frontal avalancheux, la boue tend à se déposer en couche au fond. Durant les inondations, de nombreuses rivières à lit sableux transportent des concentrations de charge de lessivage suffisamment élevées pour rendre l'eau de la rivière plus lourde que l'eau stagnante. Dans ce cas, l'écoulement de la rivière, chargé de boue, plonge pour former un courant de turbidité au fond. Un article associé présente un modèle numérique 1D de formation de delta. Dans ce modèle fluvial, la précipitation en avalanche et le dépôt du courant de turbidité sont liés par une formulation faisant intervenir une frontière mobile. Ici, ce modèle est comparé à deux expériences de propagation de delta. L'expérience révèle une interaction curieuse entre les trois éléments du modèle : la progradation de la couche supérieure enterre la couche de fond et pousse son point amont toujours plus vers l'aval, le dépôt de fond, quant à lui, soulève le pied du dépôt frontal augmentant ainsi le taux de progradation du front lorsque le sable se déverse de la couche supérieure. Le modèle numérique de l'article associé capte cette interaction en introduisant un minimum de paramètres d'ajustement. La description morphodynamique de delta obtenue est très proche de celle qui est observée par exemple dans le delta du Colorado, USA, là où il atteint le lac Mead.

*Keywords:* Experiments on delta progradation; numerical simulations; sand-mud interface; bed evolution; initial mixing coefficient; fall velocity.

## 1 Introduction

A 1-D numerical model of delta progradation is presented in a companion paper to the present one, Kostic and Parker (2003). The model applies to sand-bed rivers carrying mud as wash load, and as such is abstracted to two grain sizes, one for sand and one for mud. The sand is deposited fluvially in the topset, and by avalanching at a specified slope in the foreset. The mud is carried into deep water by a plunging turbidity current, where it deposits to form a bottomset. Here the model is tested against two laboratory experiments.

## 2 Experimental apparatus and procedure

The two experiments reported here were carried out at St. Anthony Falls Laboratory, University of Minnesota, USA in a flume that was specifically designed for the study of turbidity currents (e.g. Garcia, 1993). The flume is 0.304 m (1 ft) wide, 0.76 m deep and 12.8 m long, and has glass walls which facilitate flow visualization. At the downstream end of the flume is a large damping tank. Turbidity currents fall from the flume into the damping tank, from which the turbid water can be vented from a bottom drain. Sediment-free makeup water is added at the

top of the tank, and water surface elevation is maintained by a standpipe in the tank. This configuration allows the experimental modeling of continuous turbidity currents over an extended period of time with no reflection from the downstream end and a suppressed tendency for the ambient water above the current to become polluted with sediment-laden water.

Only a reach of 7.0 m at the downstream end of the flume was used for the experiments. This reach is shown in Figure 1. The inerodible bed of the channel had a slope  $S_b$  of 0.012 except for a steeply sloping ski-jump configuration at the upstream end of the reach. Water and sediment were fed into the flume at a point just upstream of the apex of the ski-jump, upstream of which a vertical wall partitioned the experimental reach from the rest of the flume. A grid with 10 cm increments was drawn on the right glass wall looking downstream in order to facilitate the measurement of bed profiles. This grid extended over 5.3 m of the study reach. The flume was filled with standing water to a depth of about 0.41 m before commencing each of the experiment.

Water was supplied to the upstream end of the study reach from a mixing tank with a volume in excess of 2000 l. This mixing tank was filled with fresh water for the initial part of each experiment, and was filled with a slurry composed of fresh water and silica flour for the final part of each experiment. The silica flour was white in color and composed predominantly of silt sizes, and so is referred to as “white silt” here. A propeller kept the white silt in suspension in the mixing tank. The water or slurry discharged into the flume at an indentation just upstream of the crest of the ski jump, which served as a stilling basin. In addition to silica flour, sand was fed into the flume using a bulk screw feeder. The feed point was immediately adjacent to the invert from which the water or slurry discharged. This material is referred to as “black sand” in reference to its color. The delivery rate of water or slurry from the mixing tank to the flume was controlled with a valve, and set to a specified value by means of weighing of samples. The delivery rate of black sand was controlled by a dial on the screw feeder, and again set to a specified value by means of weighing of samples.

The black sand and white silt were chosen to represent the “sand” and “mud” components of the numerical model of the companion paper, Kostic and Parker (2003). The black sand was an angular black siliceous byproduct of the burning of coal with a specific gravity of  $2.60 \text{ g/cm}^3$  (submerged specific gravity  $R_S$  of 1.6) and a median size  $D_S$  of  $420 \mu\text{m}$ . The white silt was an angular powder with a specific gravity of  $2.65 \text{ g/cm}^3$  (submerged

specific gravity  $R = 1.65$ ). Two grades of white silt were used. In Experiment 1 material with a median size  $D_M$  of  $24.2 \mu\text{m}$  was used; in Experiment 2 the median size  $D_M$  was  $40.8 \mu\text{m}$ .

The grain size distributions for the black sand and the two grades of white silt are given in Figure 2. As can be seen from that figure, the black sand was well sorted. A small but noticeable fraction of the sand, however, consisted of thin flakes and curls which were considerably more mobile than the rest of the sand. The white silt was more poorly sorted. 17% of the white silt (SCS 106) used in Experiment 1 was coarser than  $62.5 \mu\text{m}$  and thus in the sand range, and 6% of the material was finer than  $1 \mu\text{m}$ . 38% of the white silt (SCS 250) used in Experiment 2 was coarser than  $62.5 \mu\text{m}$ , and 5% was finer than  $1 \mu\text{m}$ . In both cases, the “white silt”, although predominantly in the silt sizes, includes significant fractions of material in the sand and clay sizes. It should be pointed out that none of the clay sizes consisted of mineral clay, but were rather chemically inert fragments of ground silica flour.

Each experiment was commenced with sediment-free water emanating from the mixing tank, into which black sand was mixed in from the screw feeder. This black sand was allowed to form a prograding deltaic deposit in the flume with a clearly-defined fluvial topset and avalanching foreset. The black sand was too coarse to form a bottomset, instead covering the bottom of the flume downstream of the toe of the foreset with a discontinuous dusting of thin flakes and curls. Progradation continued until the toe of the foreset had migrated well beyond the base of the ski jump shown in Figure 1.

Upon establishment of a delta composed solely of black sand, each experiment was terminated and the water in the mixing tank was filled with a prescribed quantity of white silt. The experiment was then recommenced with an inflow of slurry from the mixing tank and black sand from the screw feeder. The feed rate of black sand was maintained at its previous value. The mixing tank was allowed to drain over a period lasting from 13 to 15 min, during which time approximately 1400 l of slurry was delivered to the flume. At the end of this period the experiment was halted, the mixing tank was filled with white silt and water and the experiment recommenced. Each such flow event is called a “run” here. Experiment 1 consisted of 8 runs with white silt (Runs 1-T1

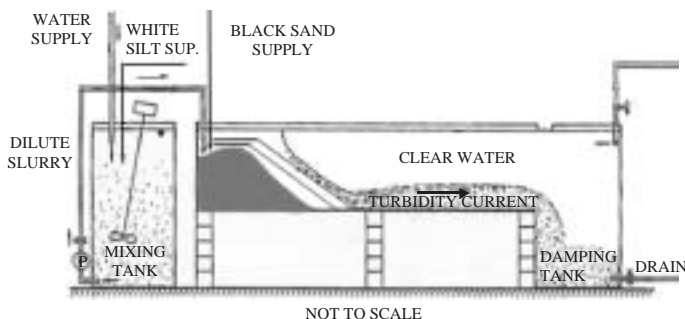


Figure 1 Schematic of the experimental facility.

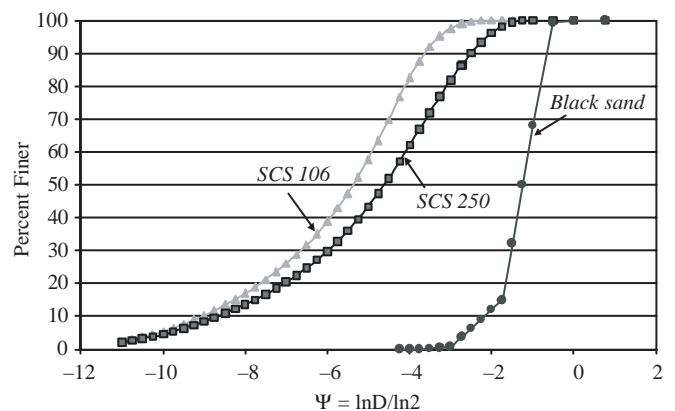


Figure 2 Grain size distributions of black sand and white silt used in experiments on sand-mud delta progradation.

to 1-T8) in addition to the initial period of deposition of pure black sand. In the case of Experiment 2 there were 6 runs with white silt (Runs 2-T1 to 2-T6). The white silt in each run insured the formation of a well-developed plunging turbidity current.

The design flow discharge  $Q_f$  of water or slurry in the experiments was 2.0 l/s. The design volume concentration  $C$  of white silt in the slurry of both experiments was 0.0239, corresponding to a feed rate of 127.2 g/s. In the case of Experiment 1, the design feed rate of black sand was 14.1 g/s, so that during Runs 1-T1 to 1-T8 the black sand would constitute 10% of the incoming sediment by weight. In the case of Experiment 2, the design feed rate of black sand was reduced to 6.69 g/s, so that during Runs 2-T1 to 2-T6 the black sand would constitute 5% of the incoming sediment by weight. As is reported below, these design values were not precisely achieved, but were achieved within a reasonable degree of approximation.

Data acquisition included the following. The discharge of water or slurry were monitored and adjusted from time to time, as was the discharge from the screw feeder. Slurry samples were taken from time to time in order to determine the concentration of white sand. Water surface elevations were monitored from the grid on the flume wall. Profiles of bed deposition were obtained by drawing colored lines on the glass wall of the flume and extracting data from the grid. At the end of each run, the centerline of the deposit was profiled with a point gage. The relative lack of three-dimensionality in the deposit meant that bed profiles obtained from the side walls were, when averaged over bedforms, good representations of the centerline bed profiles as well. Video footage and still photographs were taken to document both the progress of each experiment and the final configuration. The water was allowed to clarify before documenting the final configuration. Coal powder with a specific gravity of 1.35 was added from time to time in order to allow for visualization of the turbidity current. The deposit was sampled at the end of each experiment.

Measurements of neither turbidity current velocities nor suspended sediment concentrations in the turbidity current were taken during the experiments.

### 3 Experimental observations

Table 1 lists the design values, average measured values and standard deviation of the measured values for flow discharge of water/slurry  $Q_f$ , volume concentration of white silt in the slurry  $C$  and mass feed rate of black sand for Experiments 1 and 2. It can be seen that the values achieved were close to the design

values, and that it was possible to hold them relatively constant during the course of each experiment.

Also included in Table 1 are measurements of the concentration  $C_{amb}$  of suspended sediment in the ambient water above the turbidity current, determined from a sample taken 4 min after the end of Run 1-T8 and a sample taken 3 min after the end of Run 2-T6. At the beginning of each run with white sand the water was fairly clear, with only a small amount of white silt polluting the ambient standing water from the previous run. The ambient water was quite cloudy at the end of each such run. Most of this cloud, however, was associated with a relatively low concentration of the finest material in the white silt. The ambient concentrations listed in Table 1 are on the order of a tenth of the inflow concentrations of white silt, suggesting that the ambient water was not too severely polluted by the end of each run to substantially suppress the turbidity currents.

*Experiment 1.* The black sand delta was allowed to prograde in the absence of white silt for the first 95 min of the run. A view of the black sand delta just after the commencement of the first turbidity current run is given in Figure 3. The topset of the deposit was emplaced by a thin fluvial flow with a depth of about 1.5 cm. The black sand was observed to move mostly as an intense layer of bedload, with little suspension. The flow was slightly Froude-supercritical, as evidence by a weak undular hydraulic jump at the top of the foreset. The foreset developed by avalanching at a consistent slope angle near  $35.7^\circ$ , a value that was found to be very close to the angle of repose for the black sand. This portion of the experiment was termed Run 1-T0.



Figure 3 Establishment of a delta composed solely of black sand in Experiment 1. The flow is from left to right. The squares on the glass wall of the flume, which are  $10\text{ cm}^2$ , provide scale for this and other figures below.

Table 1 Design and average measured values, and standard deviations for some model input parameters.

EXP #	$Q_w$ (l/s)			$G_S$ (g/s)			$C$			$C_{amb}$
	Design	Avg	StDev	Design	Avg	StDev	Design	Avg	StDev	
1	2	1.9463	0.04917	14.0744	12.1811	0.17788	0.0239	0.0219	0.00085	0.002484
2	2	1.9914	0.08591	6.6668	6.1467	0.16572	0.0239	0.0228	0.00162	0.002021

Eight runs, i.e. Runs 1-T1 to 1-T8 were performed by running the slurry containing white silt over the delta. The input of black sand was held to the value prevailing during Run 1-T0. Each run produced a turbidity current which plunged just downstream of the top of the delta and then ran out the length of the flume. The plunge point varied in time, but was typically located at a point corresponding to a third of the distance down the foreset. In Figure 4a the turbidity current is made visible by the addition of coal powder. These currents were observed to be essentially depositional. Their effect was to (a) lower the slope angle of the foreset and (b) deposit a bottomset downstream of the toe of the foreset. This bottomset extended the length of the flume, indicating that a significant amount of white sand was swept out of the flume by the turbidity currents.

The topset, foreset and bottomset created at the end of Experiment 1 can all be seen in Figure 4b. It is apparent in the image

that there is a substantial amount of white silt in the topset and foreset, and some black coal in the bottomset. In order to interpret this it must be recalled that 17% of the white silt used in this experiment was actually in the sand range. It can be computed from Table 1 that for every unit of black sand fed in 1.5 units of white silt that was actually in the sand range was fed in. In addition, the black coal contained some flakes and curls of shards that were quite mobile. This notwithstanding the reasonably distinct division between (dark) topset and foreset and (light) bottomset is readily apparent.

Figure 4b reveals the interaction between the topset, foreset and bottomset. The topset and foreset are seen to be overriding antecedent bottomset material, so pushing the upstream end of the bottomset downstream. The buildup of the bottomset at the base of the foreset under the constraint of constant water surface

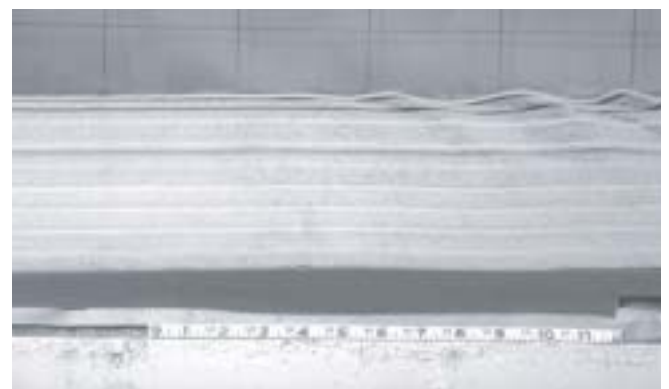
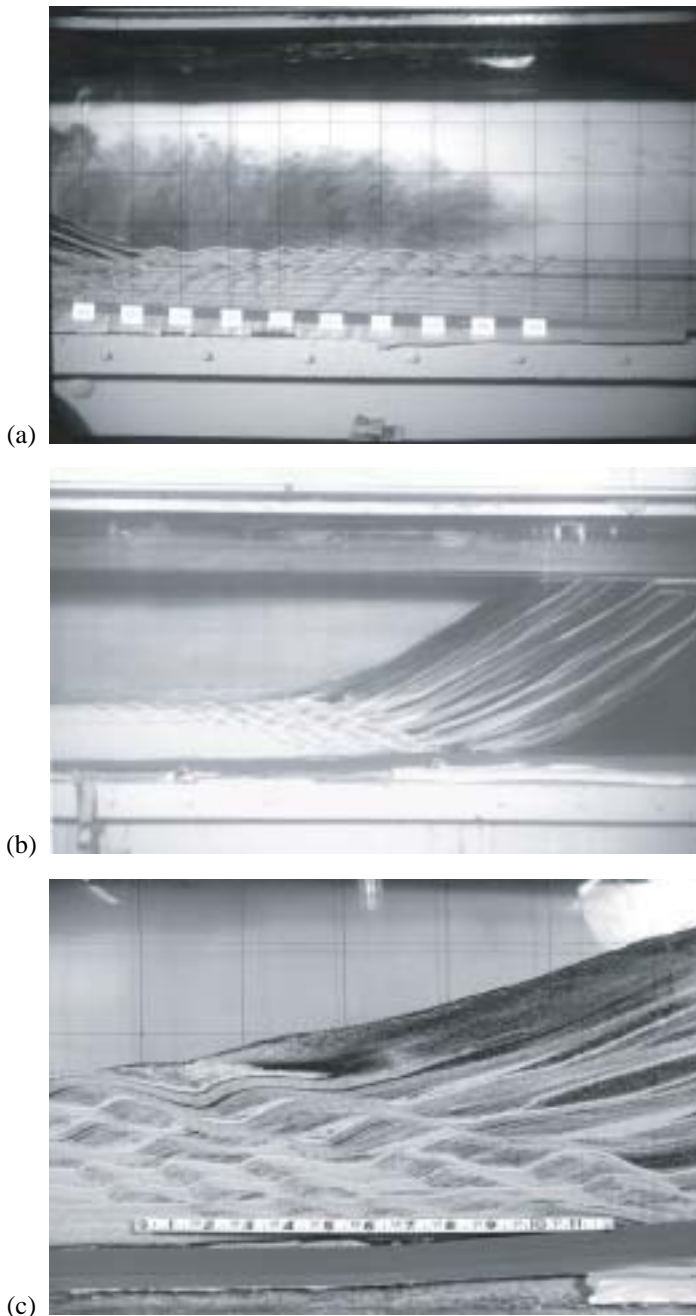


Figure 4 (a) Longitudinal propagation of tracer coal in a turbidity current over the bottomset bed just before the end of Experiment 1. The flow is from left to right. (b) Fluvial delta produced at the end of Experiment 1. The flow was from right to left. (c) Expanded view of moving boundary between the foreset, which predominantly consists of black sand, and the bottomset, which is nearly all white silt. The flow was from right to left. (d) A view from the top of the flume at downstream-migrating bedforms. The flow was from top to bottom. (e) A view from the side at downstream-migrating bedforms, illustrating how they peter out downstream. The flow was from right to left.

elevation reduces the height of the foreset, thus increasing the rate of progradation of the foreset for the same rate of delivery of sand at the top.

An expanded view of the toe of the foreset at the end of Experiment 1 is given in Figure 4c. The turbidite deposited by each of the eight runs is readily apparent in the image in terms of a thin, very white deposit capping each turbidite. This cap consisted of the finest material in the white silt at the end of each run. This material was deposited slowly from the water column at the end of the run. Also evident in the image are downstream-migrating bedforms downstream of the toe of the foreset. A view looking down at these bedforms is given in Figure 4d. They eventually petered out downstream, as shown in Figure 4e.

Measured profiles of the foresets at the end of the feeding of black sand only, and also at the end of each run are given in Figure 5. The passage of turbidity currents over the foreset reduced the foreset slope angle from  $35.1^\circ$  at the end of the part of the experiment in which only black sand was fed, i.e. Run 1-T0, to an average of  $28.8^\circ$  for all runs in the presence of white silt but Run 1-T1. This effect is in accordance with the predictions of Kostic *et al.* (2002). In addition, the presence of an overpassing turbidity current occasionally triggered slide events on the foreset. Measured bed profiles for the entire deposit at the end of each run are shown in Figure 6a. Again the distinction between topset, foreset and bottomset is readily apparent.

Average values for the fluvial flow depth  $h_f$ , bed slope  $S_f$ , friction coefficient  $C_f$  and Froude number  $Fr$  over the topset for Experiment 1 are given in Table 2. Here  $C_z$  and  $Fr$  are computed as

$$C_z = \frac{Q_f}{Bh_f\sqrt{gh_fS_f}} \quad Fr = \frac{Q_f}{Bh_f\sqrt{gh_f}} \quad (1a,b)$$

where  $Q_f$  denotes the flow discharge of the slurry,  $B$  is the flume width and  $g$  denotes the acceleration of gravity. The parameters in Table 2 were determined from data taken in the presence of a turbidity current. It can be seen that the flow during Runs 1-T1 to 1-T8 was supercritical, as it was during Run 1-T0.

*Experiment 2.* The progress of this experiment was similar to that of Experiment 1. The black sand delta was allowed to prograde out for six hours, so defining Run 2-T0. During this period the fluvial flow over the topset was observed to be slightly Froude-subcritical. After this the runs with white silt were commenced. Figure 7a shows a view of the deposit toward the end of

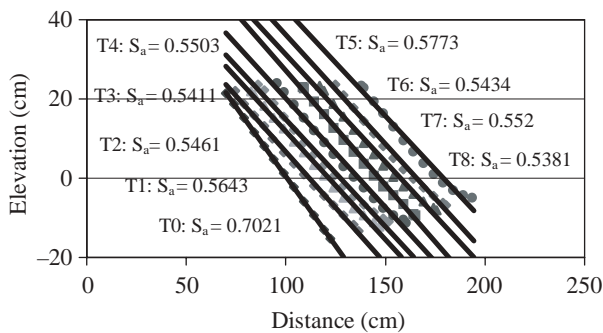


Figure 5 Measured profiles of the foreset at the end of Run 1-T0, and at the end of Runs 1-T1 to 1-T8.

the experiment. Coal powder has been added to allow visualization of the plunging turbidity current. The deposit is very similar to that of Experiment 1, except for two important differences. The topset and foreset in Figure 7a are seen to be much whiter than those of Figure 4b for Experiment 1. This is due to the fact that 38% of the white silt used in Experiment 2 was in the sand sizes, as opposed to 17% for Experiment 1. It can be computed from Table 1 that for every one unit of black sand fed into Experiment 2, 7.4 units of white silt that was actually in the sand range were fed in. This notwithstanding, the boundary between the toe of the foreset and the upstream end of the bottomset is again distinct.

The bedforms beyond the toe of the bottomset were longer and higher than those observed in Experiment 1, perhaps because of the coarser median size of the white silt. As in Experiment 1, these bedforms petered out downstream, as shown in Figure 7b.

Figure 8 shows the profiles of the foreset at the end of the part of the experiment with black sand only, and at the end of runs 2-T1 to 2-T6. In the absence of white sand the slope angle of the foreset was observed to be  $35.0^\circ$ . The average slope angle with overriding turbidity currents at the end of all runs with white silt but Run 2-T1 was  $29.2^\circ$ . Thus in Experiment 2 the reduction of the slope angle of the foreset was less than that observed in Experiment 1. This can be ascribed to the coarser grade of silt used in Experiment 2, which led to weaker turbidity currents.

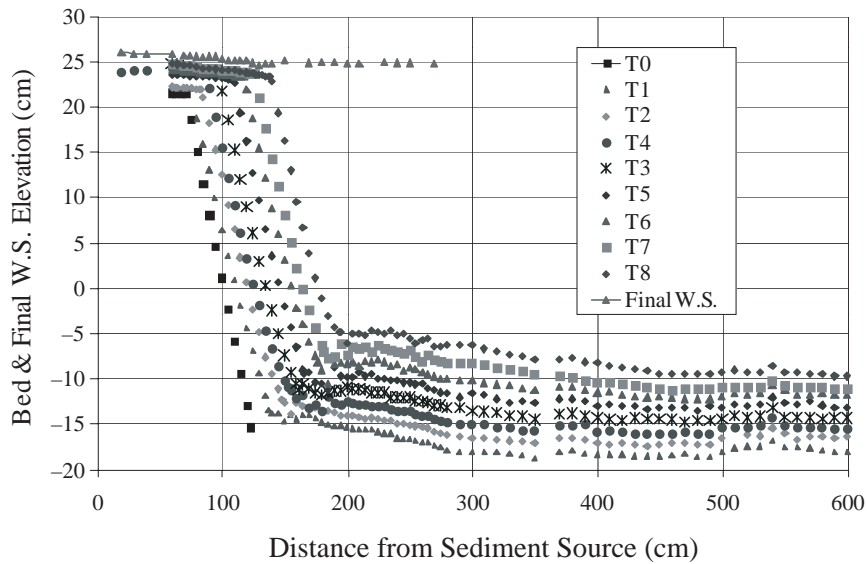
Bed profiles measured at the end of Runs 2-T0 to 2-T6 are shown in Figure 9a. The profiles are similar to those of Experiment 1, with the exception that the each bottomset turbidite thins much more rapidly in the downstream direction in the case of Experiment 2. This is at least partly a consequence of the fact that the white silt used in Experiment 2 has a much coarser median size ( $40.8 \mu\text{m}$  versus  $24.2 \mu\text{m}$ ).

Average values for the fluvial flow depth  $h_f$ , bed slope  $S_f$ , friction coefficient  $C_f$  and Froude number  $Fr$  over the topset for Experiment 2 are given in Table 2. These parameters were determined from data taken in the presence of a turbidity current. It can be seen that the flow during Runs 2-T1 to 2-T6 was slightly supercritical, as opposed to the slightly subcritical flow observed during Run 1-T0.

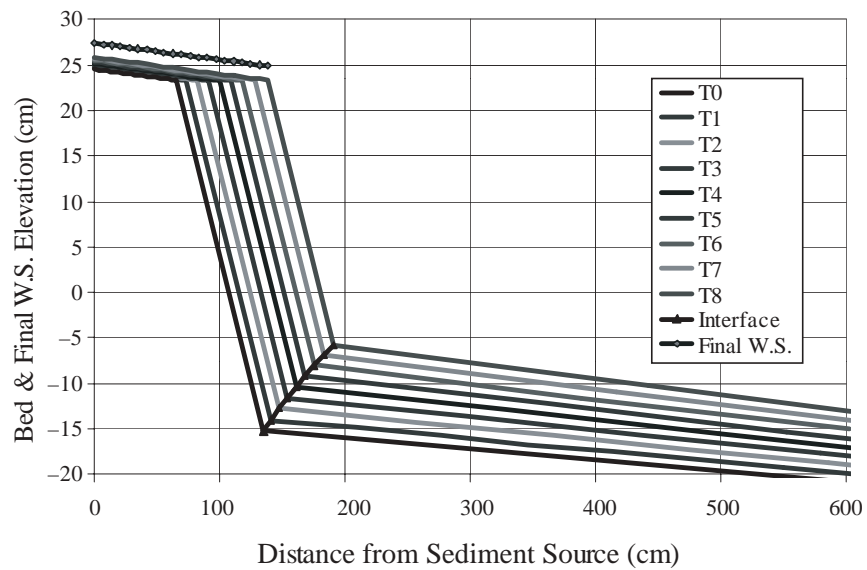
## 4 Numerical simulation of the experiments

### 4.1 Input parameters

The numerical model presented in the companion paper, Kostic and Parker (2003) was tested against the results of Experiments 1 and 2. The input parameters required for the numerical model can be divided into those for the fluvial submodel and those for the turbidity current model. The fluvial submodel uses the following input parameters: water-sediment slurry discharge per unit width  $q_w = Q_f/B$ , Chezy coefficient  $C_f$ , median diameter of sand  $D_S$ , submerged specific gravity for sand  $R_S$ , sand porosity  $\lambda_S$ , initial slope  $S_{f0}$  of the fluvial bed, volume sand feed rate per unit width  $q_{S0}$ , initial position of the top of the foreset deposit  $f_0$ , initial elevation of the toe of the foreset deposit  $\eta_{B0}$ , water surface elevation of the lake or reservoir  $Z_l$ , avalanche slope  $S_a$



(a)



(b)

Figure 6 (a) Measured bed profiles for Experiment 1 on sand-mud delta progradation. (b) Numerical simulation of Experiment 1 ( $c_D = 0.01$ ,  $\gamma = 1.5$ ).

Table 2 Calibration of the friction coefficient.

EXP #	$h_f$ (cm) Avg	$S_f$ Avg	$Fr$	$C_f$
1	1.55	0.01896	1.05649	0.01698
2	1.62	0.01260	1.01168	0.01231

and the coefficient  $\alpha$  in the Engelund–Hansen fluvial bed material transport relation (Engelund and Hansen, 1972) introduced in the companion paper, Kostic and Parker (2003). In the case of simulations at typical field scale, for which the Froude number of the river flow is well below unity, the initial elevation of the top of the foreset  $\eta_{T0}$  must be specified as well. In the present case, however, the flows were either slightly subcritical (Run 2-T0) or slightly supercritical (all other runs). In this case  $\eta_{T0}$  is computed iteratively from the specified water surface elevation, the approximation of normal flow in the river and the flow depth

determined from the relation for the hydraulic jump at the topset–foreset transition, as described in the companion paper.

The turbidity current submodel is here implemented for the case of an unstratified ambient water body. It requires the following input parameters: depth  $h_0$  of the turbidity current immediately after the plunge point, velocity  $U_0$  immediately after the plunge point, volumetric concentration  $C_0$  after the plunge point, turbidity current bottom friction factor  $c_D$ , fall velocity of mud  $v_M$ , submerged specific gravity of mud  $R$ , mud porosity  $\lambda$ , and initial slope  $S_0$  of the bottomset deposit.

#### 4.2 Normalized grain size distributions

As noted above, in both Experiments 1 and 2 a significant amount of white silt was deposited in the topset and foreset. The reason for this is easily seen from Figure 2. The finest size in the black sand was about  $88 \mu\text{m}$ . Both grades of white silt in Figure 2 contain a significant fraction (though less than 50%) of material that is

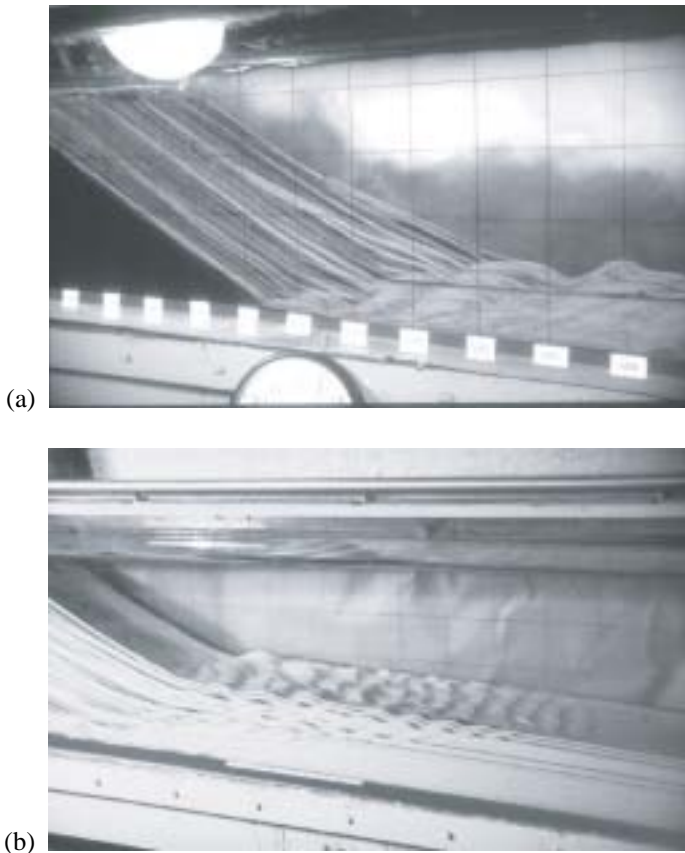


Figure 7 (a) Delta with a plunging turbidity current running over the foreset deposit right before the end of Experiment 2. The flow is from left to right. (b) A view of downstream-migrating bedforms at the end of Experiment 2. The flow was from left to right.

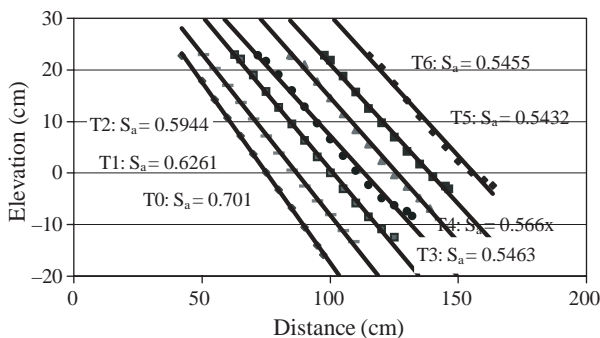


Figure 8 Measured profiles of the foreset at the end of Run 2-T0, and at the end of Runs 2-T1 to 2-T6.

coarser than  $88 \mu\text{m}$ . Since about 90% of the sediment introduced in Runs 1-T1 to 1-T8 and about 95% of the sediment introduced in Runs 2-T1 to 2-T8 consisted of white silt, it is apparent that a substantial fraction of white silt was in fact sand in a size range overlapping with the black sand.

Because of this overlap it was necessary to renormalize the size distributions of white silt so as to remove the coarse tail from the “mud” feed and add it to the “sand” feed. This was done from considerations of mass balance applied to the sediment in the topset–foreset zone. The fractions of black sand and white silt deposited in this zone between two specified times were measured. Although a detailed comparison of grain size distributions

was not performed, the white silt in question was observed to be noticeably coarser than that deposited in the bottomset. The volume of white silt in the topset–foreset zone between the specified times was converted to a mass using a measured deposit porosity, so yielding a fraction of the white silt that acted as if it were black sand. This fraction was used in conjunction with Figure 2 to obtain a cutoff size for white silt, such that material coarser should be treated as “sand” and included with the black sand, and material finer should be treated as “mud.”

The renormalized grain size distributions for “sand” and “mud” are shown in Figures 10a and b for Experiments 1 and 2, respectively. For the Experiment 1 the median size  $D_S$  for normalized “sand” was found to be  $339.2 \mu\text{m}$ , while the median size  $D_M$  for the normalized “mud” was  $22.3 \mu\text{m}$ . For Experiment 2 it was found that  $D_S$  was equal to  $236.3 \mu\text{m}$  and  $D_M$  was equal to  $31.2 \mu\text{m}$ .

In the case of the fine white grade of silt (*SCS 106*) used in Experiment 1 the fraction of white silt that deposited in the topset–foreset zone was found to be 4.7%, resulting in a cutoff size of  $105 \mu\text{m}$ . This resulted in a normalized feed rate of “sand” of  $17.6 \text{ g/s}$ , a normalized feed rate of “mud” of  $110.1 \text{ g/s}$  and a ratio  $\kappa$  of sand feed to total feed of 0.86 rather than the design value of 0.9. In the case of Experiment 2 the corresponding values are as follows: fraction white silt in the topset–foreset: 13.4%; cutoff size:  $151 \mu\text{m}$ ; normalized “sand” feed rate:  $22.3 \text{ g/s}$ ; normalized “mud” feed rate:  $104.1 \text{ g/s}$  and  $\kappa = 0.83$  rather than the design value of 0.95. In implementing the numerical model the unadjusted feed rate of black sand was used to simulate Runs 1-T0 and 2-T0; in all other cases the normalized feed rates of “sand” and “mud” were used.

In addition to the above parameters, it is necessary to determine porosities for implementing the Exner equation of sediment continuity. In the case of foreset deposits of black sand only,  $\lambda_S$  was measured to be 0.404. In the case of bottomset deposits of the finer white silt (*SCS 106*)  $\lambda$  was found to be near 0.515; in the case of the coarser white silt (*SCS 250*) it was found to be 0.444. The actual porosity of the topset–foreset deposits in the presence of feed of white silt were estimated to be close to 0.417.

#### 4.3 Calibration of friction and transport coefficients

The dimensionless Chezy coefficient of bed resistance for the fluvial zone  $C_Z$  was calculated from the known flow discharge per unit width  $q_w$ , the measured values of topset depth  $h_f$  and topset slope  $S_f$  given in Table 2 and the assumption of normal (steady, uniform) flow. Thus  $C_Z$  and the resistance coefficient  $C_f$  are given as

$$C_Z = \frac{q_w}{h_f \sqrt{g h_f S_f}} \quad C_f = (C_Z)^{-2} \quad (2a,b)$$

For the Experiment 1  $C_Z$  was found to be 7.688, and for Experiment 2  $C_Z$  was found to be 9.052. The corresponding values of  $C_f$  are reported in Table 2 along with the Froude numbers  $Fr$ .

The coefficient  $\alpha$  in the Engelund–Hansen fluvial sediment transport relation (Engelund and Hansen, 1972) has a standard

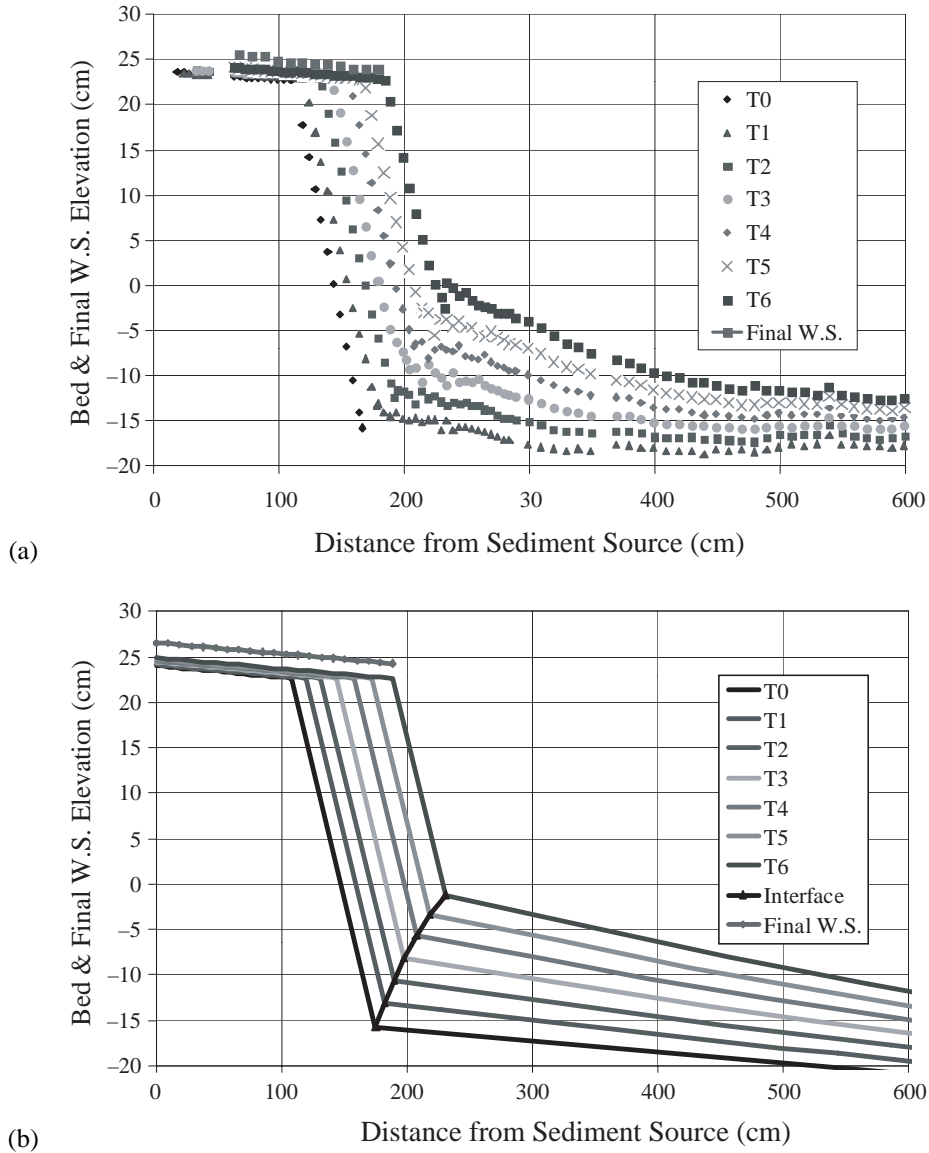


Figure 9 (a) Measured bed profiles for Experiment 2 on sand-mud delta progradation. (b) Numerical simulation of Experiment 2 ( $c_D = 0.02$ ,  $\gamma = 1.0$ ).

value of 0.05. In light of the scatter characteristic of fluvial sediment transport relations, the value of  $\alpha$  used in the numerical simulations was calibrated using the normalized “sand” feed rate and the measured values pertaining to fluvial flow of Table 2. That is,  $\alpha$  was computed from the relation

$$\alpha = \frac{q_{s0} D_s}{C_z^2 \sqrt{g h_f S_f}} \left( \frac{R_s}{h_f S_f} \right)^2 \quad (3)$$

obtained from Eq. (40) of the companion paper.

In the case of Experiment 1  $\alpha$  was found to be 0.06033 for black sand only (Run 1-T0) and 0.07044 for normalized “sand” (Runs 1-T1 to 1-T8). In the case of Experiment 2  $\alpha$  was found to be 0.05773 for black sand only (Run 2-T0) and 0.11494 for normalized “sand.” Except for the last of these numbers the deviation from the standard value of 0.05 is not unacceptably large when white silt was added.

As measurements of the flow velocity distributions of the turbidity currents were not taken, it was necessary to estimate the turbidity current bottom friction factor  $c_D$ . This value was

determined from a best fit between experimental data and numerical prediction, and assigned a constant value of 0.02. This value is in the range of values previously reported for laboratory experiments on turbidity currents (e.g. Parker *et al.*, 1987).

#### 4.4 Plunging

The turbidity current velocity  $U_0$ , depth  $h_0$ , and volume concentration  $C_0$  immediately downstream of the plunge point were calculated from relations suggested by Akiyama and Stefan (1984) for plunging over a steep slope. The parameters determined in this way are presented in Table 3. Since the initial mixing coefficient  $\gamma$  was not measured during experiments, it was determined from a relation proposed by Farrell and Stefan (1988):

$$\begin{cases} \gamma = 0, & Fr_n \leq 0.7 \\ \gamma = 0.5(Fr_n - 0.7), & Fr_n > 0.7 \end{cases} \quad (4)$$

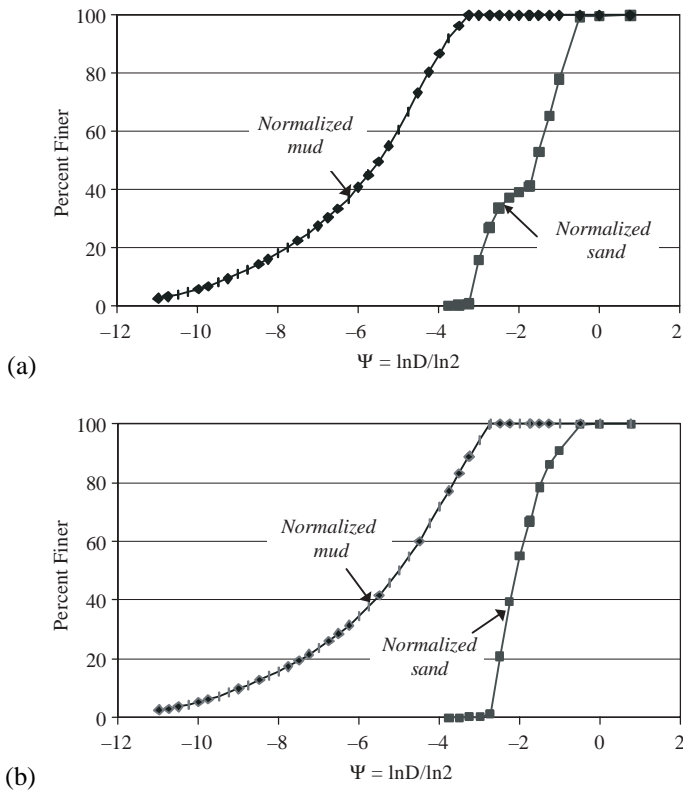


Figure 10 Normalized grain size distributions of model sand and mud. (a) for Experiment 1. (b) for Experiment 2.

Table 3 Input parameters for the turbidity current submodel.

EXP #	$c_t$	$\gamma$	$h_0$ (m)	$U_0$ (m/s)	$C_0$
1	0.01	1.5	0.11	0.143	0.00851
1	0.02	1.0	0.09	0.141	0.01053
1	0.05	0.5	0.07	0.143	0.01334
2	0.01	1.5	0.12	0.136	0.00796
2	0.02	1.0	0.10	0.138	0.00986
2	0.05	0.5	0.08	0.138	0.01251

Here  $Fr_n$  denotes normal densimetric Froude number given by the relation

$$Fr_n = \left( \frac{S_2 S_a}{c_t} \right) \quad (5)$$

where  $S_a$  is the avalanche slope,  $c_t$  is the total foreset friction coefficient and  $S_2$  is a shape factor, which was estimated to be near 0.99 by Garcia and Parker (1993) for turbidity currents in the same flume as used for the present experiments.

Equation (5) is intended to be used for estimating the mixing coefficient in reservoirs with parallel or gently diverging side-walls. Farrell and Stefan (1988) applied the above relation to calculate the mixing coefficient for a case for which  $Fr_n$  was equal to 1.16. The predicted value of  $\gamma = 0.23$  was found to be in disagreement with the experimental value of  $\gamma = 0.1$ . Thus, in the calculation of mixing coefficients presented in Table 1 Eq. (5) was multiplied by a correction factor equal to 0.1/0.23. The total friction factor  $c_t$  in (5) is again imprecisely known. As a result

three reasonable estimates were tested in performing simulations. These estimates, along with the resulting values for  $\gamma$  are shown in Table 3.

#### 4.5 Further assumptions and approximations

The following additional assumptions and approximations were introduced in numerical simulations. The water surface elevation  $Z_l$  of the flume was taken to be constant during the course of each experiment, even though there were slight oscillations due to the necessity to adjust a drain valve at the downstream end of the flume during the period between runs. The feed rates of normalized “sand” and “mud” were kept constant during each run, using the values for black sand only in Runs 1-T0 and 2-T0 and the normalized values for the other runs. In addition, water or slurry discharge per unit width  $q_w$  was kept constant. These constant values were determined based on averages of the measurements. The average measured values and associated standard deviations are reported in Table 1.

The avalanche slope  $S_a$  used in each experiment was equated to the average value for Runs 1-T1 to 1-T8 in Experiment 1 and Runs 2-T1 to 2-T6 in Experiment 2. As was reported above, the prevailing value of  $S_a$  for the case of the black sand only (Runs 1-T0 and 2-T0) was higher than for the other runs. This effect was accounted for in the model by the use of a short adjustment time in order to satisfy mass balance.

#### 4.6 Results

The numerical model was implemented for each experiment using various scenarios to test the sensitivity of the model. The input parameters which remained invariant for each experiment were  $q_w$ ,  $R$ ,  $R_S$ ,  $\eta_{B0}$ ,  $\lambda$ ,  $\lambda_S$ ,  $S_0$ ,  $S_a$ ,  $Z_l$ , normalized  $D_M$  and normalized  $D_S$ . The numerical simulations proceed as follows. In order to predict the progradation of the fluvial delta consisting entirely of black sand in Runs 1-T0 and 2-T0 the model was run over the antecedent inerodible bed with then normalized “mud” feed rate  $q_M = 0$ . In Run 1-T0 the sand delta was allowed to prograde for 112.5 min. This progradation time includes the duration of the experiment (95 min) and the adjustment time (17.5 min), that accounts for the change of avalanche slope between Run 1-T0 and Runs 1-T1 to 1-T8. In Run 2-T0 the black sand delta was similarly allowed to prograde for 408 min. The predicted patterns of progradation are shown in Figures 11a and b.

The profiles obtained in Figures 11a and b were used as the initial profiles for simulating Runs 1-T1-8 and 2-T1-6, respectively. In the case of Experiment 1 the simulation continued for 114 min, corresponding to the total duration of all eight runs. In the case of Experiment 2 the simulation correspondingly continued for 87 min.

In the case of Experiment 1 the best fit for the runs with mud was obtained for the choices  $c_D = 0.01$  and  $\gamma = 1.5$ . The experimental measurements for all eight runs are summarized in Figure 6a, and the numerical predictions are presented at the same scale in Figure 6b. The agreement is seen to be quite good.

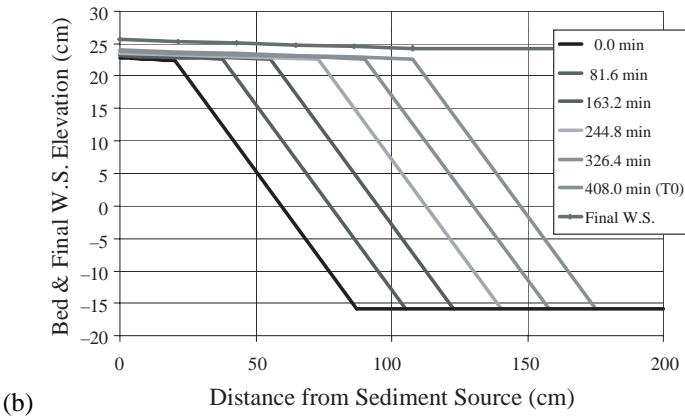
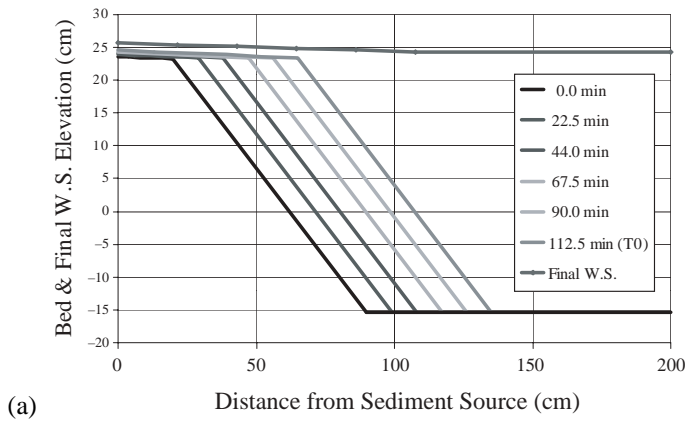


Figure 11 Numerical predictions on progradation of black sand delta. (a) for Experiment 1. (b) for Experiment 2.

In the case of Experiment 2 the best fit for the runs with mud was obtained for the choices  $c_D = 0.02$  and  $\gamma = 1.0$ . The experimental measurements for all six runs are summarized in Figure 9a, and the numerical predictions are presented at the same scale in Figure 9b. The agreement is also seen to be good, although not as good as that of Experiment 1. The main source of discrepancy is the degree of concavity in the bottomset profiles, with the simulations showing less concavity than the data. This effect may be due in part to the abstraction of many grain sizes in the depositional turbidity current to a single grain size.

The effects of variation of the turbidity current bottom friction factor  $c_D$  and initial mixing coefficient  $\gamma$  were analyzed in the case of Experiment 1. A change in this parameter from 0.01 to 0.02 resulted in only a slight decrease in the bottomset elevation, as well as a slight downstream displacement of the foreset–bottomset interface to the right. More precisely, the streamwise position of the interface was displaced a negligible amount, whereas the elevation of the interface was depressed by up to 3%. Increasing  $c_D$  from 0.01 to 0.05 still resulted in negligible downstream displacement of the interface, but the elevation is depressed by as much as 13%.

A change in the initial mixing coefficient  $\gamma$  proved to have a much more pronounced effect on the bottomset near the toe of the foreset. Lower values of  $\gamma$  were associated with a higher concentration of mud at the inflow boundary of the turbidity current, leading to a bottomset that built up more rapidly and a foreset–bottomset interface that migrated with a steeper angle

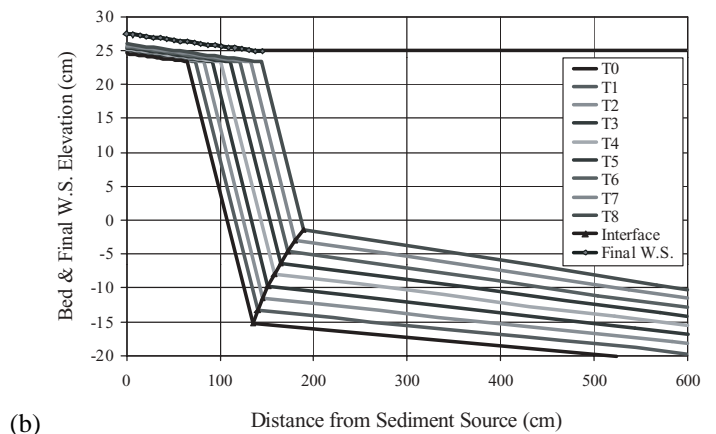
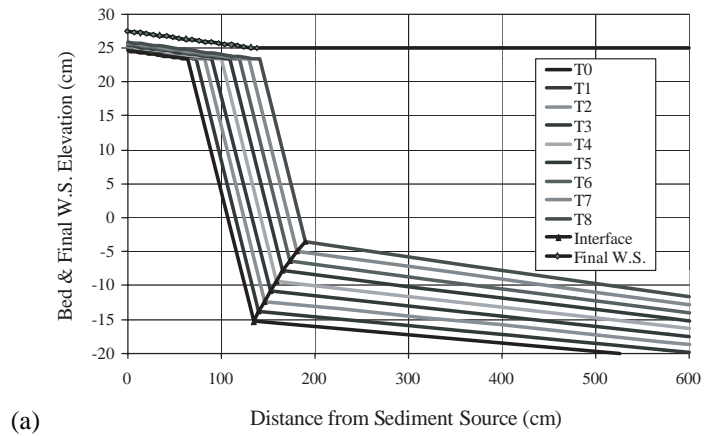


Figure 12 Effect of the mixing coefficient and bottomset friction factor on the foreset–bottomset interaction. (a)  $c_D = 0.02$ ,  $\gamma = 1.0$ . (b)  $c_D = 0.05$ ,  $\gamma = 0.5$ .

to the horizontal. The combined effects of variation of initial mixing coefficient and turbidity current friction factor on the deposits can be seen by comparing Figures 6b with Figures 12a and b. Since the effect of varying the friction factor  $c_D$  is negligible over the range 0.01 to 0.05, most of the differences between the figures can be attributed to variation in initial mixing coefficient  $\gamma$ .

The effect of mud fall velocity  $v_M$  was investigated in the case of Experiment 2 by means of increasing  $D_M$  at constant  $R$ . An increase in the grain size of mud from  $31.2 \mu\text{m}$  to  $35 \mu\text{m}$  resulted in a decrease in the streamwise progradation of the foreset–bottomset interface of up to 1% and an increase in bottomset elevation of up to 77%. An increase in mud grain size from  $D_M$  from  $31.2 \mu\text{m}$  to  $40 \mu\text{m}$  results in a decrease in interface progradation of as much as 2.5% and an increase in interface elevation of up to 185%. These changes may be seen by comparing Figures 13a–c. In all three cases the initial mixing coefficient  $\gamma$  was taken to be 1.5, as opposed to the value of 1.0 used in Figure 9b. It thus can be concluded that a higher mud fall velocity results in a bottomset that aggrades more rapidly, so reducing the height of the foreset and increasing the rate of foreset progradation. A comparison of Figures 9b and 13a reveals that a value of  $\gamma$  of 1.0 provides a much better fit between the simulated and experimental values than a value of 1.5.

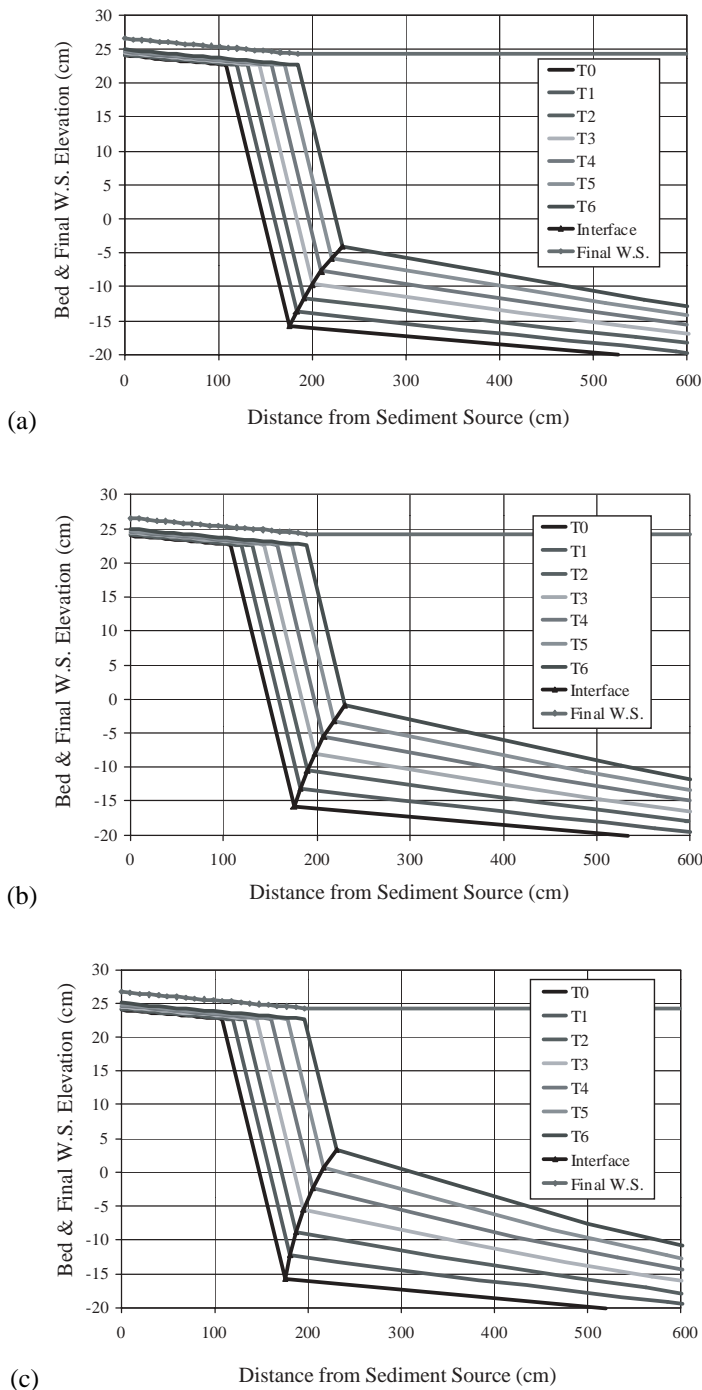


Figure 13 Effect of mud diameter on resulting deposits ( $c_D = 0.01$ ,  $\gamma = 1.5$ ). (a)  $D_M = 31.2 \mu\text{m}$ ; (b)  $D_M = 35 \mu\text{m}$ ; (c)  $D_M = 40 \mu\text{m}$ .

## 5 Conclusions

The numerical model of prograding deltas described in the preceding companion paper (Kostic and Parker, 2003) was tested against two experiments on sand-mud delta progradation. Comparison of the numerical predictions and experimental data illustrates the ability of the numerical model to capture the co-evolution of sandy topset and foreset deposits with muddy bottomset deposits. This reasonable agreement was achieved with a minimum of parameter adjustment within the constraints of the data available. The evolution of the foreset–bottomset interface observed in the experiments and successfully simulated in the

model is reminiscent of that observed not only in the field-scale simulations of the companion paper, but also that observed in the delta of the Colorado River in Lake Mead (Figure 3b of the companion paper.)

The fluvial part of the numerical model proved to be sensitive to the choices of Chezy friction coefficient  $C_z$  and standing water surface elevation  $Z_l$ . In the case of standing water surface, this sensitivity was observed in the experiments themselves, where even slight increases and decreases in water surface elevation were found to affect the topset.

The turbidity current part of the model was found to be sensitive to the choice of the initial mixing coefficient  $\gamma$ . This parameter influenced the rate of aggradation of the bottomset and foreset–bottomset interaction predominantly through its effect on the volumetric concentration of mud immediately after the plunge point. Variation in the mud fall velocity  $v_M$  proved to have a similar impact on bottomset aggradation. As opposed to uncertainties associated with the choice of the mixing coefficient, the range of realistic fall velocities can be determined relatively correctly.

Other parameters that introduce uncertainties in the numerical modeling are: porosity ( $\lambda_S, \lambda$ ), the coefficient  $\alpha$  in Engelund–Hansen relation and bottomset friction factor  $c_D$ . Of these parameters, the most difficult to estimate is  $c_D$ . The numerical model, however, proved to be relatively insensitive to increases in  $c_D$  of up to 400%.

Generally, because of the time scale associated with fluvial and turbidity current processes, the latter have the most significant impact on the short-term interaction between deposits of the experiments analyzed here.

Two ways in which the model can be improved are (a) generalization of the model to multiple grain sizes and (b) generalization to a configuration in which the deltaic topset deposits flare out in the transverse direction (Parker *et al.*, 1998). The authors are presently pursuing the latter generalization.

This work is the result of research sponsored by the Minnesota Sea Grant and the Office of Naval Research STRATAFORM program. The Minnesota Sea Grant College Program is supported by the NOAA Office of Sea Grant, United States Department of Commerce, under grant no. NOAA-NA86-RG0033. The U.S. Government is authorized to reproduce and distribute reprints for government purposes, not withstanding any copyright notation that may appear hereon. This paper is journal reprint no. JR489 of the Minnesota Sea Grant College Program.

## Notation

- $B$  = flume width
- $C$  = volumetric concentration of white silt in the slurry
- $C_{amb}$  = volumetric concentration of suspended sediment in the ambient water
- $C_f$  = topset friction factor ( $=C_z^{-2}$ )
- $C_0$  = volumetric concentration of white silt immediately after the plunge point
- $C_z$  = dimensionless Chezy resistance coefficient
- $c_D$  = bottomset friction coefficient

$c_t$  = total foreset friction coefficient  
 $D_S, D_M$  = median diameters of sand and mud respectively  
 $Fr$  = Froude number of open-channel flow  
 $Fr_n$  = normal densimetric Froude number  
 $f_0$  = initial position of the top of the foreset deposit  
 $g$  = acceleration of gravity  
 $G_S$  = mass feed rate of black sand  
 $h_0$  = turbidity current depth immediately after the plunge point  
 $h_f$  = depth of the fluvial flow  
 $R, R_S$  = submerged specific gravity of mud and sand respectively  
 $S_a$  = avalanche slope  
 $S_0, S_{f0}$  = initial slope of the bottomset and topset bed respectively  
 $S_2$  = shape factor  
 $S_f$  = topset slope  
 $Q_f$  = flow discharge of the slurry  
 $q_{S0}$  = volume discharge per unit width of sand  
 $U_0$  = turbidity current depth immediately after the plunge point  
 $v_M$  = mud fall velocity  
 $Z_l$  = water surface elevation of the lake or reservoir  
 $\alpha$  = coefficient in the Engelund–Hansen transport relation  
 $\gamma$  = initial mixing coefficient  
 $\eta_{T0}$  = initial elevation of the top of the foreset deposit  
 $\eta_{B0}$  = initial elevation of the toe of the foreset deposit

$\kappa$  = feed ratio  
 $\lambda, \lambda_S$  = porosity of mud and sand deposits respectively

## References

1. AKIYAMA, J. and STEFAN, H. (1984). "Plunging Flow into a Reservoir: Theory", *J. Hydr. Engrg.*, 110(4), 484–499.
2. FARRELL, G.J. and STEFAN, H.G. (1988). "Mathematical Modeling of Plunging Reservoir Flows", *J. Hydr. Res.*, 26(5), 525–537.
3. GARCIA, M. (1993). "Hydraulic Jumps in Sediment-Driven Bottom Currents", *J. Hydr. Engrg.*, 119(10), 1–24.
4. GARCIA, M. and PARKER, G. (1993). "Experiments on the Entrainment of the Sediment into Suspension by a Dense Bottom Current", *J. Geophys. Res.*, 98, 4793–4807.
5. KOSTIC, S., PARKER, G. and MARR, J. (2002). "Role of Turbidity Currents in Setting the Foreset Slope of Clinofolds Prograding into Standing Fresh Water", *J. Sedimentary Res.*, 72(3), 353–362.
6. KOSTIC, S. and PARKER, G. (2003). "Progradational Sand-Mud Deltas in Lakes and Reservoirs: Part 1. Theory and Numerical Modeling", *J. Hydr. Res.*, 41(2), 127–140.
7. PARKER, G., GARCIA, M., FUKUSHIMA, Y. and YU, W. (1987). "Experiments on Turbidity Currents Over an Erodible Bed", *J. Hydr. Res.*, 25, 123–147.
8. PARKER, G., PAOLA, C., WHIPPLE, K. and MOHRIG, D. (1998). "Alluvial Fans Formed by Channelized Fluvial and Sheet Flow: Theory", *J. Hydr. Engrg.*, 24(10), 1–11.